Short lifetimes in ^{30}P

P. Tikkanen, J. Keinonen, and R. Lappalainen
University of Helsinki, Accelerator Laboratory, Hämeentie 100, SF-00550 Helsinki, Finland

B. H. Wildenthal
Drexel University, Philadelphia, Pennsylvania 19104
(Received 24 February 1987)

Mean lifetimes of levels in ^{30}P have been measured by application of the Doppler-shift attenuation method and the ^{29}Si(p,γ)^{30}P reaction. Values or limits were determined for the lifetimes of 27 bound levels below the excitation energy of 6.1 MeV; the lifetimes of eight of these levels are reported for the first time. The targets were prepared by implanting ^{29}Si into Ta backings in order to provide effective stopping of recoils. The Monte Carlo method and experimental stopping powers were used in the Doppler-shift attenuation analysis. The experimental transition strengths are compared with the predictions of recent shell-model calculations.

I. INTRODUCTION

The present work is a continuation of our systematic study of short lifetimes in the *sd*-shell nuclei.[1–4] Recent work on large-basis multishell wave functions for the *sd*-shell nuclei[5–7] has revealed the necessity of reliable and consistent lifetime data for the $M1$ and $E2$ transition strengths, since these provide the most sensitive tests of the wave functions. As a self-conjugate nucleus, ^{30}P provides a good opportunity to deduce pure isovector and isoscalar components in $M1$ and $E2$ transitions.

Previous to this experiment, lifetime values in ^{30}P from several Doppler-shift attenuation (DSA) studies[8–11] have been reported. However, due to the use of media with rather long slowing-down times [e.g., SiO_2, SiO (Refs. 11–15), and Al (Refs. 16–18)] and application of the slowing-down theory[19] without sufficient experimental validation, the extracted lifetime values have large uncertainties and there is considerable scatter in the results of different measurements. In three other brief reports no information is available on the method of the DSA analysis.[20–22] The use of experimental stopping powers has been shown to yield excellent agreement between lifetime values obtained in low[9] and high[10] recoil velocity DSA measurements. This emphasizes the need of a new, systematic study of ^{30}P lifetimes which includes use of experimentally determined stopping powers.

This paper describes lifetime measurements in ^{30}P which utilize the ^{29}Si(p,γ)^{30}P reaction and the improved DSA method developed in our laboratory.[4] The essential improvement over other, older measurements in this work and the previous studies from our laboratory[9,23] is the use of targets in which ^{29}Si is implanted into Ta, thus producing a high stopping power. Further improvement was gained by using experimentally known stopping powers in the DSA analysis. With this technique, the lifetimes of the excited states in ^{30}P could be determined to accuracies sufficient to permit extraction of transition strengths which can be compared meaningfully with theoretical values. In addition, this and our previous[1–3] studies with detailed and similar DSA measurements and analysis yield consistent lifetime data in different *sd*-shell nuclei.

II. EXPERIMENTAL ARRANGEMENTS

The 2.5 MV Van de Graaff accelerator of the University of Helsinki Accelerator Laboratory supplied the proton beam of about 30 μA. The beam was collimated to form a spot of 3×3 mm^2 on the target. The ^{29}Si targets, specially designed for the Doppler-shift measurements, were prepared by implanting an 8 μg/cm^2 fluence of 50 keV $^{29}Si^+$ ions into 0.4 mm thick Ta backings in the isotope separator of the same laboratory. The maximum concentration of ^{29}Si was about 20 at. %, as determined by backscattering of 2 MeV He^+ ions.

The γ-radiation was detected by a PGT 110 cm^3 Ge(Li) detector which had an efficiency of 21.8%. The energy resolution of the detection system was 2.0 keV at $E_\gamma=1.3$ MeV and 3.1 keV at $E_\gamma=2.6$ MeV. The stability of the spectrometer was checked with a ^{208}Tl γ source and the ^{40}K laboratory background. The DSA measurements were performed with the detector at angles of 0° and 90° to the beam direction and a target-detector distance of 5 cm. The corrections for solid-angle attenuation of the observed Doppler shifts were based on consideration of the primary γ-ray transitions. The recorded γ-ray spectra represent accumulated charge of 0.1–0.3 C each.

III. MEASUREMENTS AND RESULTS

The detailed γ-decay scheme study of Reinecke *et al.*[11] was used to select resonances for the DSA measurements. The resonances typically decay to several bound states. The resonances selected were those which fed the levels studied almost entirely by primary transitions. Measurements were performed on eight resonances in the range $E_p=1373$–2122 keV. In order to ensure that the $F(\tau)$ values were not affected by unknown feedings, measurements on a given level were performed at more than one resonance if sufficient population could be seen. The branching ratios for decays from bound states were taken

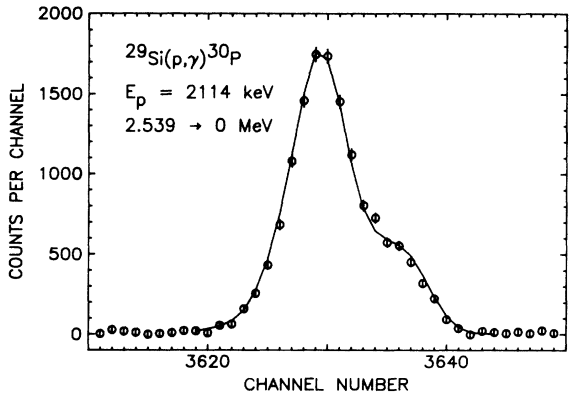

FIG. 1. Portion of γ-ray spectra recorded in the DSA measurements of the 2.539 MeV state. The dispersion is 0.70 keV/channel. The solid line is the Monte Carlo simulation of the γ-ray line shape at 0°; the fit is shown for the lifetime 205 fs. The adopted lifetime is $\tau(2.539)=202\pm31$ fs.

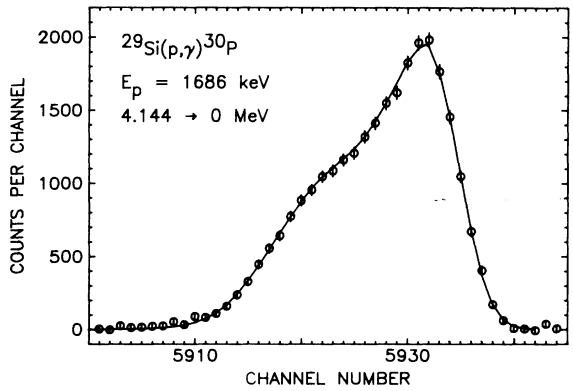

FIG. 3. As for Fig. 1, but for the 4.144 MeV state. The Monte Carlo simulation is for the lifetime 55 fs. The adopted lifetime is $\tau(4.144)=55\pm8$ fs.

from Ref. 11.

In our analysis of the γ-ray spectra accumulated in the DSA measurements, the branches and their intensities were observed to be generally in agreement with the data quoted in the literature.[11] In the analysis of the $E_p=2038$ keV resonance we obtained new branchings of 3% and 6% to the $E_x=5.509$ and 5.577 MeV levels, respectively. These values are averages from the 0° and 90° measurements. In comparison with the intensities of the secondary transitions, about 75% of the primary strength of this resonance is still unobserved. The analysis of the spectra for this $E_p=2038$ keV resonance also yielded a new decay scheme for the 5.577 MeV state; we obtain branches of (13±3)%, (39±3)%, (15±1)%, (18±2)%, and (15±2)% for the decays to the 0, 0.709, 1.455, 3.734, and 3.836 MeV levels, respectively. Only the decay to the 0.709 MeV level was known previously.[11] The branching was given to be (50±10)%, and 50% was reported to be unobserved.

In the analysis of the $E_p=1748$ keV resonance a new 3% branch to the 5.210 MeV level was seen. The 5.210 MeV state was observed to decay to the ground state with the branching of (76±3)% and to the 0.709 MeV state with the (24±3)% branch. In Ref. 11 it was reported as (60±10)% to the g.s. and 40% unobserved. The 4.941 MeV state was observed to have a (93±2)% branch to the 0.677 MeV state and a (7±1)% branch to the 1.974 MeV level [(90±10)% in Ref. 11, and 10% unobserved].

The summary of the present DSA measurements is given in Table I. The $F(\tau)$ values shown in the table are averages from at least two sets of measurements. Corrections to the quoted $F(\tau)$ values for indirect feedings were introduced where necessary. The results of the DSA measurements of the 2.539, 2.938, 4.144, 4.737, 5.506, and 5.702 MeV states are illustrated in Figs. 1–6.

The DSA analysis of the experimental $F(\tau)$ values was performed using Monte Carlo calculations.[1,4] The relevant data for the description of the stopping of the recoiling ^{30}P nuclei in Ta were taken from our earlier studies[24,25] in which the experimental stopping parameters for the nuclear (f_n) and electronic (f_e) stopping power were determined for ^{27}Al and ^{35}Cl recoiling in Ta. These studies indicate that there are no abrupt changes in the stopping power for recoiling atoms with similar Z values: $f_n=0.67\pm0.08$, $f_e=1.0\pm^{0.8}_{0.2}$ for ^{27}Al ($Z=13$), and

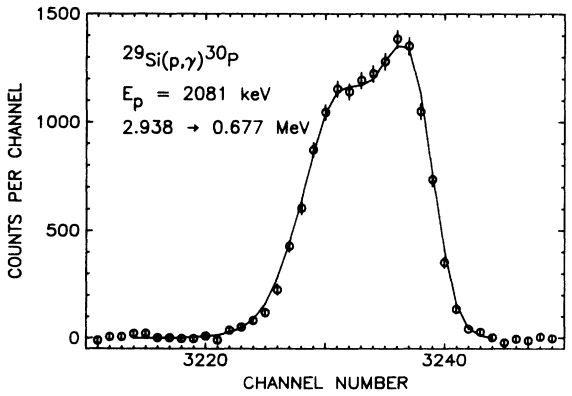

FIG. 2. As for Fig. 1, but for the 2.938 MeV state. The Monte Carlo simulation is for the lifetime 83 fs. The adopted lifetime is $\tau(2.938)=86\pm13$ fs.

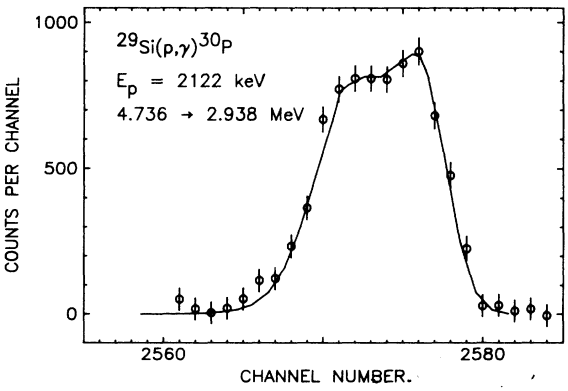

FIG. 4. As for Fig. 1, but for the 4.736 MeV state. The Monte Carlo simulation is for the lifetime 74 fs. The adopted lifetime is $\tau(4.736)=77\pm12$ fs.

TABLE I. Summary of lifetimes in ^{30}P from the present DSA analysis, and comparison with the previously known lifetimes.

				τ (fs)						
				Present[c]	Previous					
E_x (MeV)	Measurement at E_p (keV)	$F(\tau)$[a] (%)	τ[b] (fs)		Ref. 12[k]	Ref. 21[l]	Refs. 16 and 17	Ref. 20[l]	Ref. 11	Others
0.677	1373	27.0±0.5	130±4[m]	130±20			160±45	130±40	130±20	155±30[d]
										$170\pm^{220}_{80}$[e]
2.539	2038	22±3	180±30[m]	200±30	92±21	260±85	225±60	190±40		80±25[e]
	2055	21±5	220±60[m]							
	2081	23±6	205±65							
	2114	22.1±1.0	205±8							
	2122	20.0±0.8	202±4							
2.724	1373	28±9	140±60	150±20	96±15	160±20	175±55	180±40	160±25	148±22[f,k]
	1748	23.4±1.5	145±5							
	2055	25.3±1.7	160±12[m]							
	2081	29±7	155±50[m]							
	2114	29±2	143±5							
	2122	24.0±1.1	147±7							
2.840	1686	6±4	$770\pm^{1230}_{350}$[m]	610±180		790±210	1200±350	670±150	720±230	3000±1500[g,l]
	2114	11±4	$470\pm^{350}_{150}$[m]							
	2122	9±2	$600\pm^{240}_{130}$[m]							
2.938	1373	28±9	105±45[m]	86±13	37±5		95±30	115±20	65±10	70±10[f,k]
	2081	39.6±1.0	86±3							90±11[h]
										90±12[i]
										105±35[j,l]
										48±7[e]
3.019	1686	96.1±1.6	2.4±1.9	3±2		< 10	< 30	34±10	< 10	< 12[e]
	2038	94±4	< 7[m]							< 29[f,k]
	2122	89±11	< 5[m]							< 15[j,l]
3.734	1686	56±4	40±6	38±7		19±7	55±40	44±12		
	1748	62±3	36±6							
3.836	1373	58±13	42±19	52±8		44±7	34±16	83±20	45±10	
	1748	47±8	63±21							
	2038	48±6	63±14							
	2055	52±12	60±25							
	2114	57±5	47±8							
	2122	53.2±1.7	52±4							
3.927	2038	41±11	90±40	87±30		105±20	128±35	90±20		
	2055	52±20	70±40							
	2114	37±8	100±40							
4.144	1373	47±10	60±25	55±8	58±14	46±8	52±19	43±10	38±8	40±5[j,l]

TABLE I. (*Continued.*)

E_x (MeV)	Measurement at E_p (keV)	$F(\tau)$[a] (%)	τ[b] (fs)	τ (fs) Present[c]	Previous Ref. 12[k]	Ref. 21[l]	Refs. 16 and 17	Ref. 20[l]	Ref. 11	Others
	1686	50.3±0.6	54.6±1.4							22±2[e]
										25±9[f,k]
4.183	1748	93.8±4.8	3.9±1.4	3.4±1.2		<24	<20	<40	10±4	<15[j,l]
	2038	84.8±2.0	<5[m]							<20[f,k]
	2081	95±4	3.4±2.7							3.1±0.9[h]
	2114	95±3	3.2±2.0							
	2122	95±3	3.4±2.0							
4.233	2114	8±7	2200±1900	1750±950	>1200	2800±1700	740±200		>1000	>1500[e]
	2122	6±4	1600±1100							>1300[f,k]
										3100±1900[j,l]
4.298	2114	28±7	143±24	137±26			185±70			
	2122	29±8	133±20							
4.344	2038	33±8	146±24	145±30			185±50			
4.422	1748	43.4±0.8	67±2	67±10	64±8	58±6			42±12	19±8[e]
	2114	52±5	56±10							40±7[f,k]
4.468	1373	94.6±0.8	2.8±0.4	2.8±0.5	<33				<10	
4.502	1373	90±3	6.3±1.9	6.3±2.2					<10	<47[j,l]
										5±3[e]
4.627	1686	16±3	262±25	260±45	260±60		220±60		340±65	250±85[j,l]
	2055	17.3±1.9	262±32[m]							240±40[e]
										280±60[f,k]
4.736	1748	39±5	88±12	77±12					70±15	
	2038	40±3	83±9							
	2114	43±3	74±6							
	2122	41±2	77±3							
4.938	2038	90±3	6.7±2.1	6.6±2.0						<10
4.941	1748	91±2	6.2±1.3	6.2±1.6	47±20	<25				<10
5.207	1748	65±3	31±4	30±6						18±6
	2038	67±5	29±6							
5.506	2038	92.5±1.6	5.5±1.0	5.5±1.3						<10
5.509	2038	80±6	15±6	15±7						<10
5.577	2038	86±3	9±2	9±2						
5.702	2038	79±3	16±3	16±4						<10
6.095	2055	90.6±1.6	6.3±1.2	6.3±1.5						

[a]Values have not been corrected for feeding. [b]Values given are based on the $F(\tau)$ value and line shape analysis. Only statistical uncertainty is shown. [c]Values include the uncertainty in the experimental stopping power. [d]Ref. 18. [e]Ref. 23. [f]Refs. 13 and 14. [g]Ref. 22. [h]Ref. 9. [i]Ref. 10. [j]Ref. 15. [k]Uncertainty due to the slowing-down theory was not included. [l]No information on the DSA analysis was given. [m]Value has been corrected for feeding.

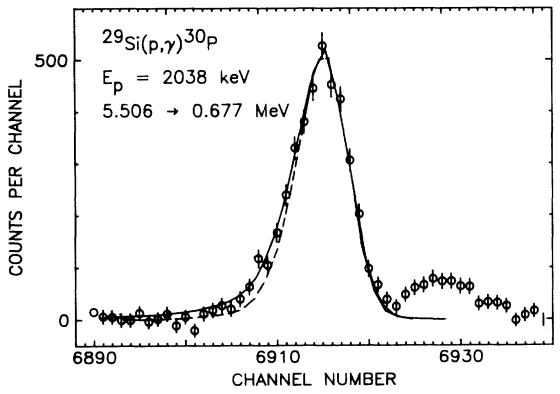

FIG. 5. As for Fig. 1, but for the 5.506 MeV state. The instrumental line shape shown by the dashed line is obtained from the primary transition $r \rightarrow 2.724$ MeV at $E_\gamma = 4857$ keV and $E_p = 2055$ keV. The Monte Carlo simulation is for the lifetime 5.5 fs. The adopted lifetime is $\tau(5.506) = 5.5 \pm 1.3$ fs.

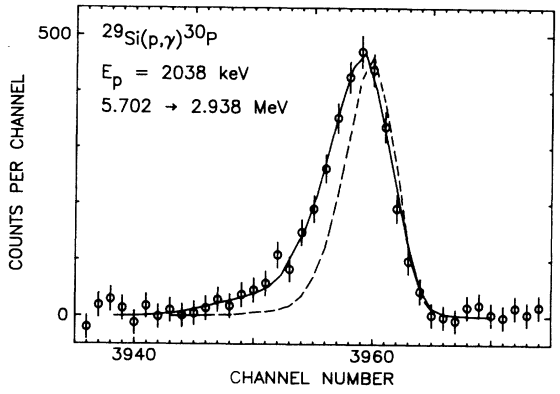

FIG. 6. As for Fig. 1, but for the 5.702 MeV state. The instrumental line shape shown by the dashed line is obtained from the primary transition $r \rightarrow 4.737$ MeV at $E_\gamma = 2828$ keV. The Monte Carlo simulation is for the lifetime 16 fs. The adopted lifetime is $\tau(5.702) = 16 \pm 4$ fs.

$f_n = 0.68 \pm 0.06$, $f_e = 1.00 \pm 0.19$ for ^{35}Cl ($Z = 17$).

The total stopping power for Si is hence taken to be

$$\left[\frac{d\epsilon}{d\rho}\right]_{\text{corr}} = (0.68 \pm 0.10)\left[\frac{d\epsilon}{d\rho}\right]_n + (1.0 \pm 0.3)\left[\frac{d\epsilon}{d\rho}\right]_e^{\text{LSS}} .$$

(LSS denotes Lindhard-Scharff-Schiøtt[19]). The enlarged error limits are assumed to take account of the uncertainty of the interpolation. The uncorrected nuclear stopping power was calculated by the Monte Carlo method, with the scattering angles of the recoiling ions derived directly from the classical scattering integral[26] and the interatomic interaction described by the Thomas-Fermi potential. The uncorrected electronic stopping power was calculated in the framework of the LSS theory.[19]

We have recently studied[4] the change of the density of the backing material which results from the implants and their effect upon the lifetimes obtained by DSA. The data indicate that at concentrations below about 20 at. % of light-ion implants any possible density changes in Ta have an insignificant effect on the lifetime values. In the present work, the proton energies were selected so that the slowing down of ^{30}P took place beyond the maximum concentration of the range profile of ^{29}Si, i.e., at concentrations below 20 at. %.

The present results for the mean lifetimes of 27 bound levels below 6.1 MeV in ^{30}P are summarized and compared with previous data in Table I. The experimental conditions of the present and previous DSA measurements are given in Table II. Excluding the two previous

TABLE II. Summary of DSA measurements for lifetimes in ^{30}P.

Work	Reaction	v/c (%)	Slow-down medium
Present	^{29}Si(p,γ)	0.18–0.23	Ta + implanted ^{29}Si (12 μg cm^{-2})
Ref. 11		0.13–0.23	evaporated enriched ^{29}SiO$_2$ (80 μg cm^{-2}) + Ta
Ref. 9		0.13–0.25	Ta + implanted ^{29}Si (4.4 μg cm^{-2})
Ref. 23		0.19–0.20	Ta + implanted ^{29}Si (2 μg cm^{-2})
Refs. 13,14		0.13–0.21	evaporated enriched ^{29}SiO (100 μg cm^{-2}) + nat. SiO + Ta
Ref. 15		0.19–0.21	evaporated enriched ^{29}SiO$_2$ (70 μg cm^{-2}) + Au
Ref. 12		0.13–0.20	evaporated enriched ^{29}SiO$_2$ (20 μg cm^{-2}) + Au
Ref. 21		0.19–0.20	not given
Refs. 16,17	^{27}Al(α,n)	0.67–0.90	Al foil (1.66 mg cm^{-2}) + Au
Ref. 18		0.61	evaporated Al (10–50 μg cm^{-2}) + C (50,125 μg cm^{-2}) + Ta
Ref. 22		0.69–0.86	not given
Ref. 10	^{3}He(^{28}Si,p)	3–4	Al, Zr, Nb, and Au + implanted ^{3}He

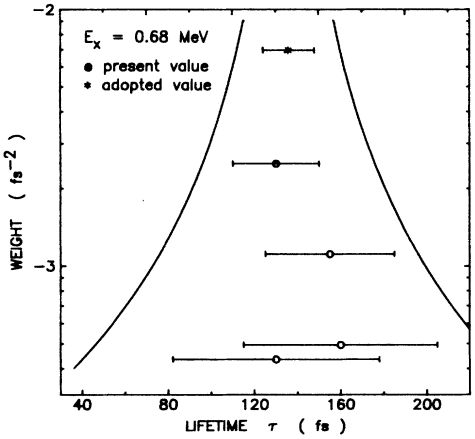

FIG. 7. A plot of the weights of lifetime measurements of the 0.677 MeV state vs lifetime value. The weight of a measurement is taken as $(\Delta\tau)^{-2}$, where $\Delta\tau$ is the quoted uncertainty. If the uncertainty due to the stopping power is not included in $\Delta\tau$ in the original paper, an uncertainty of 20% is added in quadrature for the comparison with other values. Two contours at τ(adopted)$\pm 2(\Delta\tau)$ are also shown.

studies reported from our laboratory, in which the same procedures as in the present work were used to obtain the lifetimes of the 2.938 and 4.183 MeV states[9] and in which the experimental range data were used to correct the value of the nuclear stopping power,[23] all previous studies used nuclear stopping powers obtained from the LSS theory,[19] with the large-angle scattering correction as given by Blaugrund.[27]

The corrected electronic stopping powers[28] used in Refs. 11, 13, and 14 have a negligible effect on the DSA analysis of those low-recoil-velocity measurements. The measured electronic stopping cross sections for ^{31}P ions in C were used in Ref. 18 to scale the stopping cross sections for ^{30}P in Al by a factor of 1.16 ± 0.20. The imperfect knowledge of the slowing-down mechanism has been taken into account by increasing the error limits of the extracted lifetimes by 25% (Refs. 16 and 17) or 15% (Ref. 11) in quadrature. No experimental details are available in Refs. 20–22. Accurately known electronic stopping powers were used by Alexander *et al.*[10]

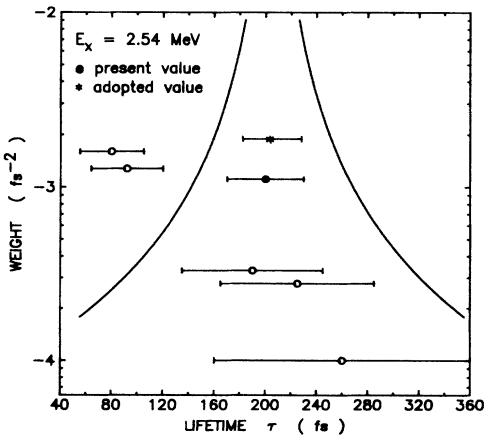

FIG. 8. As for Fig. 7, but for the 2.539 MeV state.

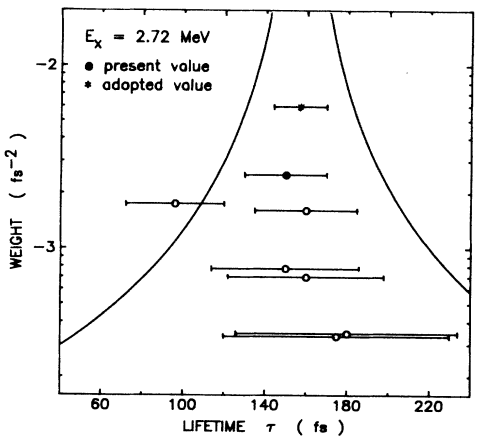

FIG. 9. As for Fig. 7, but for the 2.724 MeV state.

The lifetimes of the 0.677 2.539, 2.724, 2.938, and 4.144 MeV levels have been measured several times. The previous results, along with the present measurements, are displayed in Figs. 7–11 according to the method of Alexander and Forster.[29] In these figures the value of the weight of the measurement is plotted on a logarithmic scale as a function of the lifetime value. The weight is assumed to be $(\Delta\tau)^{-2}$, where $\Delta\tau$ is the quoted uncertainty on the lifetime measurement. However, in cases for which only statistical errors have been reported in the literature or for which no information is available on the procedures of the DSA analysis, an uncertainty of 20% has been added in quadrature to the quoted uncertainty in order to make comparison on an equal basis with values from those measurements where the uncertainty due to the stopping power is included. The reference value is the adopted value and contours at $\pm 2(\Delta\tau)$ are centered at this value. The composite lifetime values obtained by this method from the present and previous data are used in Table III.

IV. DISCUSSION

The results of our present lifetime measurements were combined with previous measurements as described to ob-

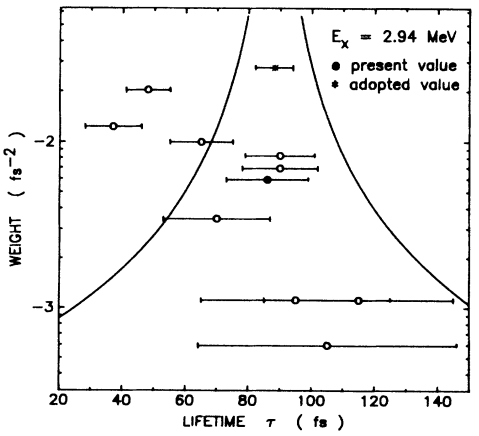

FIG. 10. As for Fig. 7, but for the 2.938 MeV state.

TABLE III. Experimental transition strengths of positive parity states in ^{30}P and their comparison with recent shell model calculations.[a]

$(E_x)_i$ (keV)			$(E_x)_f$ (keV)		τ ($\times 10^n$s)			Branching ratio (%)		$\lvert M(M1)\rvert$ μ_N			$\lvert M(E2)\rvert$ (e fm^2)	
Expt.	Theor.	$(J,T,$ No.$)_i$	Expt.	$(J,T,$No.$)_f$	Expt.	Theor.	n	Expt.	Theor.	Expt.	Theor[b]	Theor[c]	Expt.	Theor.
677	693	011	0	101	136±12	150	−15	100	100	1.16±0.05	1.069	1.008		
709	644	102	0	101	48.6±1.1	78	−12	100	100	<0.10	0.090	0.087	<16.8	5.5
1455	1491	201	0	101	6.5±0.8	3.2	−12	95.6±0.3	96.9	0.106±0.008[d]	0.141	0.124	4.1±0.5[d]	6.6
			709	102				4.4±0.3	3.1	<0.068	0.016	0.035	<11	9.3
1974	2061	301	0	101	3.44±1.20	2.2	−12	45.0±0.3	32.5				5.0±0.9	4.8
			709	102				55.0±0.3	64.7				16.8±2.9	17.2
2539	2510	302	0	101	205±23	252	−15	96.6±0.9	94.5				16.0±0.9	14.7
			709	102				3.0±0.2	4.7				6.4±0.4	6.9
			1974	301				0.4±0.1	0.5	<0.21	0.312	0.249	<44	2.8
2724	2461	202	0	101	157±13	256	−15	97.3±0.4	95.1	0.148±0.014[e]	0.132	0.079	11.2±1.8[e]	11.3
			709	102				2.7±0.4	3.8	<0.08	0.066	0.045	<4.6	3.4
2840	2973	303	0	101	720±100	1034	−15	18±2	4.5				2.8±0.3	1.0
			709	102				53±2	58.3				9.8±0.8	6.9
			1455	201				29±2	33.8	<0.25	0.073	0.059	<21	15.0
2938	3003	211	0	101	88±6	50	−15	16.4±0.8	1.7	0.14±0.03[f]	0.058	0.173	<1.6[f]	0.7
			677	011				33.2±1.0	17.9				15.0±0.7	14.9
			709	102				5.4±0.6	2.9	<0.13	0.111		<7	0.8
			1455	201				44.4±1.0	67.2	0.65±0.04[g]	1.056	1.132	<9[g]	1.4
			1974	301				0.6±0.2	5.9	<0.15	0.635	0.090	<18	0.3
3019	3131	103	677	011	3±2	3.5	−15	100	98.0	2.1±0.7	1.828	1.532		
3734	3737	104	0	101	32±6	19.0	−15	51±5	10.3	<0.23	0.141	0.106	<7	4.2
			677	011				29±3	87.6	0.233±0.025	0.758	0.710		
			1455	201				11±2	1.1	<0.22	0.090	0.071	<12	5.3
			2938	211				9±2	0.5	<0.98	0.495	0.657	<150	2.0
3836	4113	203	709	102	49±5	28	−15	22.1±1.0	25.8	<0.20	0.115	0.065	<7.8	7.6
			1455	201				9.3±1.1	5.7	<0.20	0.022	0.021	<10	8.1
			2938	211				68.6±1.2	60.1	<2.35	2.095	1.854	<310	0.5
3927	4285	304	1455	201	100±15	50	−15	22±3	9.9	<0.24	0.141	0.094	<12	5.5
			2938	211				78±3	72.5	<1.79	1.656	1.367	<220	0.1
4183	4243	212	0	101	3.2±0.7	2.1	−15	12.5±0.7	15.2	<0.39	0.519	0.514	<11	0.8
			677	011				1.3±0.3	0.7				5.6±1.3	4.9
			709	102				73.8±1.0	70.7	1.25±0.19[h]	1.432	1.129	<4[h]	1.3
			1455	201				4.4±0.9	4.0	<0.44	0.507	0.314	<19	0.1
			1974	301				3.8±0.3	3.4	<0.56	0.663	0.700	<30	0.8
			2539	302				4.2±0.3	5.0	<0.92	1.145	1.103	<67	0.2
4344	4584	501	1974	301	155±25	172	−15	95±2	92.9				27.1±2.5	21.7
			2539	302				5±2	6.5				12.3±2.6	9.4
4422	4358	204	0	101	54±6	40	−15	96.5±1.5	65.6	0.054±0.014[i]	0.003	0.004	6.4±3.0[i]	6.5
			709	102				3.5±1.5	18.8	<0.06	0.103		<1.9	4.0
			2938	211				0	13.0		0.608			0.8
4468	4778	012	0	101	2.8±0.5	0.24	−15	91.8±1.3	96.4	0.46±0.04	1.446	1.297		
			709	102				8.2±1.3	3.4	0.18±0.03	0.337	0.376		
4502	4903	111	0	101	5.8±1.8	1.3	−15	41±3	25.8	0.35±0.07[j]	0.530	0.622	2.8±1.2[j]	3.1

TABLE III. (*Continued*).

$(E_x)_i$ (keV)			$(E_x)_f$ (keV)		τ ($\times 10^n$s)			Branching ratio (%)		$\lvert M(M1)\rvert$ μ_N			$\lvert M(E2)\rvert$ (e fm^2)	
Expt.	Theor.	$(J,T,$ No.$)_i$	Expt.	$(J,T,$No.$)_f$	Expt.	Theor.	n	Expt.	Theor.	Expt.	Theor[b]	Theor[c]	Expt.	Theor.
			709	102				4.0±0.7	1.0	<0.15	0.130		<4.6	0.4
			1455	201				55±3	71.3	0.75±0.15[k]	1.562	1.495	<3[k]	1.3
4736	4862	305	0	101	74±9	84	−15	10.0±0.7	51.0				1.8±0.2	3.6
			709	102				7.0±0.6	1.1				2.3±0.2	0.7
			1455	201				12.5±2.4	35.4	<0.14	0.049	0.033	<5.0	7.2
			2938	211				68.4±1.7	0.8	<0.80	0.078	0.049	<53	0.2
4938	4931	105	677	011	6.6±2.0	2.4	−15	82.8±3.1	82.3	0.53±0.09	0.878	0.544		
			2938	211				17.2±1.9	14.4	<0.75	1.196	0.877	<45	1.3
5207	5574	306	0	101	24±6	28	−15	76±3	61.5				6.9±1.0	4.8
			709	102				24±3	26.5				5.6±1.0	4.3
5506	5896	106	0	101	5.5±1.3	0.4	−15	1.5±0.5	0.2	<0.053	0.035	0.020	<1.1	1.2
			677	011				96.0±0.5	93.3	0.52±0.06	1.598	1.404		
			2938	211				2.5±0.5	5.1	<0.21	0.904	0.761	<10.0	1.6
5509	5654	311	1455	201	15±7	3.9	−15	58±4	54.6	<0.48	0.881	0.662	<14.2	0.6
			1974	301				42±4	39.6	<0.50	0.933	0.700	<17.0	1.9
5577	5741	213	0	101	9±2	0.9	−15	13±3	15.7	<0.15	0.512	0.420	<3.3	1.5
			709	102				39±3	59.3	<0.33	1.201	1.194	<8.0	1.0
			1455	201				15±1	11.5	<0.26	0.690	0.462	<7.6	2.4
			1974	301					8.5		0.738			2.1
			3734	104				18±2	1.2	<0.95	0.697	0.742	<62	1.0
			3836	203				15±2	0.9	<0.95	0.838	0.919	<65	0.2

[a]Except for the mean lifetimes, the experimental data are from Refs. 8, 9, and 11.
[b]Free nucleon operator.
[c]Renormalized operator.
[d]$\delta(E2/M1)=0.22\pm0.02$.
[e]$\delta(E2/M1)=-3.0\pm0.4$.
[f]$\delta(E2/M1)=0.8\pm0.4$.
[g]$\delta(E2/M1)=0.03\pm0.03$.
[h]$\delta(E2/M1)=-0.01\pm0.08$.
[i]$\delta(E2/M1)=-19\pm8$.
[j]$\delta(E2/M1)=0.09\pm0.04$.
[k]$\delta(E2/M1)=-0.01\pm0.03$.

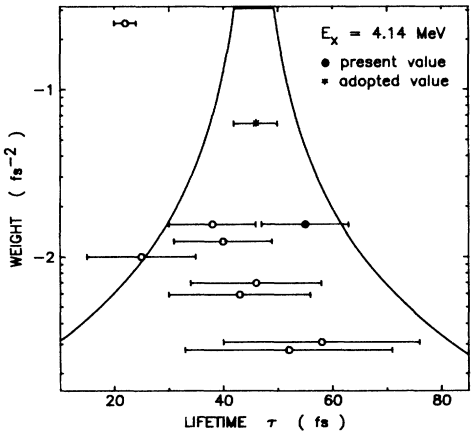

FIG. 11. As for Fig. 7, but for the 4.144 MeV state.

tain "best average values." These values are presented in Table III, along with the consensus values[30] for the low-lying states we did not address in these experiments. Also presented in this table are the experimentally determined magnitudes of the $M1$ and $E2$ matrix elements for each observed decay, as extracted from these lifetime values in combination with available branching and mixing ratios from Refs. 8, 9, and 11.

The various experimental values for the spectrum of ^{30}P are displayed in Table III in comparison with the results of shell-model predictions for excitation energies, lifetimes, branching ratios, and $M1$ and $E2$ matrix elements. These calculations are part of a comprehensive and consistent treatment of the *sd*-shell structure of all $A=17-39$ nuclei.[6,30] The initial evaluations of the results of these calculations suggest[6,30] that they yield a good accounting for the level densities of positive-parity states in the first several MeV of excitation energy in mid-*sd*-shell nuclei and that the wave functions are able to reproduce many features of the observed electromagnetic properties of low-lying states. It is thus of interest to make an extensive and intensive test of these calculations for a single nuclear system, to evaluate the degree to which the totality of the features over several MeV of excitation can be accounted for in one theoretical formulation.

The calculation of electromagnetic matrix elements from the shell-model wave functions requires the use of an $E2$ operator which is renormalized by an effective-charge model or something equivalent in order to reproduce absolute magnitudes of electric quadrupole values. We use in this work an effective charge model which incorporates harmonic oscillator single-particle radial wave functions and added charges of $0.35e$ to the model protons and neutrons. The $M1$ operator based on the magnetic moments of the free neutron and proton can be combined with the shell-model wave functions to yield $M1$ matrix elements whose absolute magnitudes are in reasonably good agreement with experimental values. Nonetheless, renormalization of the $M1$ operator for shell-model calculations is also called for by a more comprehensive theory to nuclear structure, and such a renormalization seems to improve agreement between theory and experiment on the average.

In Table III we show, in comparison with the experimental values, the shell-model predictions for level energies, lifetimes and branching ratios, and $M1$ and $E2$ matrix elements. In the case of $M1$ matrix elements we show theoretical values for both the free-nucleon and the renormalized operators. The theoretical lifetimes are calculated with the theoretical decay energies and for all theoretically allowed decays. These same calculations yield predicted branching percentages, which are compared with the experimental values without any renormalization for the fact that the experimental percentages for the observed states all add up to 100% while the corresponding theoretical percentages typically do not. Extraction of experimental values for the $M1$ and $E2$ matrix elements required knowledge of the $E2/M1$ mixing ratios in the cases where both multipolarities are allowed. For many transitions in Table III the mixing ratio is unmeasured, so that only upper bounds of the magnitudes of the matrix elements can be quoted.

The spectrum of ^{30}P provides a diverse array of electromagnetic transitions because of its juxtaposition of $T=0$ and 1 states. The $T=0$ $M1$ matrix elements are inhibited because of the cancellation which results from the opposite signs of the neutron and proton magnetic moments and have typical values in the range 0.05–0.20 μ_N. The $T=1$ $M1$ matrix elements can be much larger, with values easily ranging up to 2 μ_N. The isovector $E2$ matrix elements, on the other hand, typically are small, of the order of 1 e fm^2, as a consequence of the operator and general nuclear structure trends. The isoscalar values, which reflect shape collectivity, can range up to the order of 20 e fm^2. We will see these general features reflected in the various transitions together with structure features specific to the various individual levels.

The first excited state of ^{30}P, which occurs at 677 keV excitation energy with spin-parity-order-number values of $(J^\pi;T)_n=(0^+;1)_1$, decays to the $(1^+;0)_1$ ground state with a pure $M1$ transition. The predicted $M1$ matrix element and corresponding lifetime agree very well with experiment. The predicted small isoscalar $M1$ matrix element for the decay of the 709 keV, $(1^+;0)_2$ state to the ground state dominates the competing, moderate-sized isoscalar $E2$ component because of the small energy release factor. Agreement with experiment is satisfactory. The ground-state decay branch dominates the decay of the 1455 keV, $(2^+;0)_1$ state. Both the $M1$ and $E2$ matrix elements for the ground-state decay are predicted to be larger than observed, but the absolute differences are small relative to the typical fluctuations of the calculations, and there is good agreement between experiment and theory for the overall pattern of the decay. The decay of the 1974 keV, $(3^+;0)_1$ state proceeds to the first two $(1^+;0)$ states with comparable intensities. The predicted isoscalar $E2$ matrix elements are in good agreement with observation.

The decay of the 2539 keV, $(3^+;0)_2$ state also proceeds to the first two $(1^+;0)$ states, but in this case the ground-state branch dominates. Again, the predicted isoscalar $E2$ matrix elements agree well with the experimental results. A similar decay pattern is observed for the 2724 keV, $(2^+;0)_2$ state, and the predictions are again in good agree-

ment with experiment. In this case, both $M1$ and $E2$ components are allowed and are competitive, with the $E2$ dominating the ground-state branch and the two modes being about of equal importance in the excited-state branch. The decay of the 2840 keV, $(3^+;0)_3$ state is relatively hindered. The ground-state branch ($E2$) is quite weak, with the bulk of the decay going to the 709 and 1455 keV states. The predictions are in good agreement with observations in all details, the difference in the ground-state branching percentage resulting from a trivial difference in the very small associated $E2$ matrix element.

The decay of the 2938 keV, $(2^+;1)_1$ state is more complex than those of the lower lying levels, with measured intensity to five final states. The decays to the $(0^+;1)_1$ and $(2^+;0)_1$ states dominate both the measured and predicted decay patterns. The strong $E2$ decay to the $(0^+;1)$ state is the universal strong $2^+\rightarrow 0^+$ first-excited to ground state decay seen in all doubly even nuclei. The ^{30}P example is the analog of the ^{30}Si-^{30}S transitions. The decay to the $(2^+;0)$ state is dominated by a large isovector $M1$ transition. While both experimental and theoretical values are large, the prediction is significantly larger than experiment. The underprediction of the ground-state branching fraction would be appreciably improved by using the renormalized $M1$ matrix element which is 3 times larger than the free-nucleon value. The renormalized $M1$ value for the decay to the $(3^+;0)$ state, this time much reduced from the free-nucleon value, would also improve this branching fraction prediction.

The decay of the 3019 keV, $(1^+;0)_3$ level, both observed and predicted, proceeds entirely to the $(0^+;1)$ level at 677 keV. The predicted $M1$ element agrees within the error assigned to the experimental value. The observed decay scheme of the 3734 keV, $(1^+;0)_4$ state distributes significant intensity to four final states, those with $(J^\pi;T)_n=(1^+;0)_1$, $(0^+;1)_1$, $(2^+;0)_1$, and $(2^+;1)_1$. The predicted pattern incorrectly assigns the dominant branch to the $(0^+;1)$ state on the basis of an isovector $M1$ matrix element that is 3 times larger than the experimental value. This same matrix element also is the primary factor in the predicted lifetime being significantly shorter than the measured value.

The decay of the 3836 keV, $(2^+;0)_3$ state skips the $(1^+;0)$ ground state and proceeds to the $(1^+;0)_2$, $(2^+;0)_1$, and $(2^+;1)_1$ states. There is overall good agreement between experiment and theory for the branching fractions and individual $M1$ and $E2$ matrix elements. The renormalized $M1$ matrix elements would yield a somewhat longer lifetime than the free-nucleon value, and this would be in still better agreement with the observed value. The observed decay of the 3927 keV, $(3^+;0)_4$ state proceeds only to the $(2^+;0)_1$ and $(2^+;1)_1$ levels, in a ratio of 1 to 4. This is consistent with the predicted pattern. Again, the individual predicted matrix elements are in good agreement with the measured values, the renormalized $M1$ values yielding a better agreement with the measured lifetime than is obtained from the free-nucleon values.

The 4183 keV, $(2^+;1)_2$ state is the fourteenth positive-parity level observed in the ^{30}P spectrum. Its predicted energy is 4243 keV. Up through this excitation energy there is an unambiguous one-to-one correspondence between each of the observed ^{30}P levels and a model counterpart of the appropriate $(J;T)$ value, with differences between observed and calculated energies averaging about 150 keV. The agreement between experiment and predictions which we have noted for the decay schemes and lifetimes of the twelve states discussed so far argues that these model wave functions have a systematic and meaningful correspondence with the physical ^{30}P wave functions. The decay of the 4183 keV state provides further confirmation of this. It is, like that of the $(2^+;1)_1$ state, quite complex. Of the six observed final states, the branch to the $(1^+;0)_2$ state, at 75%, dominates. All of the many facets of the decays of this second $(2^+;1)$ state, which are predicted from the corresponding shell-model wave functions, are in excellent agreement with their experimental counterparts. Even more than the succession of agreements between theory and experiment for individual matrix elements, the fact that these ten predicted transition strengths, involving seven different wave functions, are all simultaneously consistent with experiment testifies to the power of the shell-model approach based on a realistic basis space and an empirically validated Hamiltonian. Such agreement strongly suggests that the model incorporates the dominant degrees of freedom which govern nuclear structure in this region and has correctly combined them.

The 4344 keV state, which we assume to have $(J;T)_n=(5;0)_1$, is observed to decay only to the first two $3^+;0$ states. The predicted lifetime and branching fractions agree closely with the experimental values and so, hence, do the corresponding isoscalar $E2$ matrix elements. The 4422 keV state, assumed to have $(J;T)_n=(2;0)_4$, is observed to have a lifetime which is relatively long for a state at this excitation energy. The dominant decay is to the ground state. The predicted decay is roughly consistent with the observed features. The ground-state branch is predicted to be dominated by the $E2$ component, while the predicted decay to the second $(1^+;0)$ state has similar $E2$ strength and a larger $M1$ component than the ground-state branch. These matrix elements are larger than the limits imposed from experiment, but not by amounts which are significant in the context of the normal scatter of the model values. An appreciable branch to the $(2^+;1)_1$ state is predicted which is not observed.

The observed decay pattern of the second $(0^+;1)$ state, whose measured excitation energy is 4468 keV, is similar to the predicted domination of pure $M1$ branches to the first two $(1^+;0)$ states, with the branching ratio from the renormalized operator being in even better agreement with experiment than that of the free-nucleon operator. The predicted lifetime, however, is an order of magnitude shorter than is observed. The corresponding errors in the $M1$ matrix elements are significant, and indicate defects which we presume to reside in the wave function of the $(0^+;1)_2$ state, since the two $(1^+;0)$ states have been participants in so many other, more successful, comparisons. The lifetime predicted for the $(1^+;1)_1$ state is again shorter than is observed for its experimental counterpart observed at 4502 keV excitation energy, but not by such a

large factor. The predicted branching patterns, again dominated by the $M1$ components, are similar to those observed, with the renormalized values again agreeing best with experiment. In this $(J^\pi;T)=(1^+;1)$ example, the magnitudes of the $M1$ matrix elements are systematically larger than experiment but not by amounts large enough to suggest any significant defect in the wave function.

The state observed at 4736 keV is assumed to correspond to the $(3^+;0)_5$ model state. Its measured lifetime is in agreement with prediction but its observed pattern of decay branches is inconsistent with the predicted pattern. The observed dominant branch to the 2938 keV, $(2^+;1)_1$ state is not predicted. All of the predicted $E2$ matrix elements are very small, and their deviations from the measured values are not significant. The problem arises with the $M1$ matrix element involving the $(2^+;1)$ state. It is predicted to be very small but the measured value (systematics strongly suggests that the $M1$ component dominates the relevant transition) is moderately large. This is a wave function error of the opposite sort to that observed with the $(0^+;1)_2$ state, since here we have a theoretical matrix element which is too small. With a matrix element which is predicted to be large, but too large, the error is clearly one of too strong an overlap between the two states involved, which serves to characterize the defect. In the case of theoretical matrix element which is smaller than it should be, little more can be deduced. In the present case we note that the individual one-body–transition paths are all rather weak and, in addition, the cancellation between these competing paths is almost complete.

The 4938 keV state, which we assume to correspond to the $(1^+;0)_5$ model level, is observed to decay to the lowest 0^+ and 2^+ $T=1$ states. The predicted branching ratios for this state agree with experiment, with the renormalized $M1$ matrix elements being in close agreement with the measured values. We assume that the 5207 keV state corresponds to the $(3^+;0)_6$ model state. The observed decays proceed only to the first two $(1^+;0)$ states, in accord with predictions for this state. The experimental and theoretical lifetimes and and their associated $E2$ matrix elements agree well with each other. Underlying this decay pattern are significant suppressions of other possible decay branches involving both the isoscalar and isovector $M1$ operators. We assume that the state observed at 5506 keV corresponds to the $(1^+;0)_6$ model state. The decay patterns for this pair of levels are dominated by the pure $M1$ branch to the $(0^+;1)_1$ state. The observed lifetime is 10 times longer than predicted, however. This results in relations between the observed and predicted $M1$ matrix elements which are very similar to those noted for the decay of the $(0^+;1)_2$ state. Again, we assume that the wave function defects are more logically attributed to the decaying state.

The state at 5509 keV excitation energy, which is observed to decay to the $(2^+;0)_1$ and $(3^+;0)_1$ states, is assumed to correspond to the $(J^\pi;T_n)=(3^+;1)_1$ state. Considering the uncertainty in the experimental lifetime, there is reasonably good agreement of both the relative and absolute values of the predicted $M1$ matrix elements with experiment. The state at 5577 keV excitation energy is assumed to correspond to the $(2^+;1)_3$ model state. The observed decay is complex, as was noted to be the case for the lower two $(2^+;1)$ states. The predicted branching pattern, dominated by the branch to the $(1^+;0)_1$, is qualitatively in agreement with what is observed for this state, but the predicted lifetime is an order of magnitude too small. This error is attributable to model $M1$ matrix elements for the decays to the first two $(1^+;0)$ states which are 3 times larger than the experimental limits.

The 5577 keV, $(2^+;1)_3$ state is the twenty-fourth observed level of ^{30}P to which we have postulated a model counterpart. The correspondences between observed and model levels are made on the basis of compatible spin-parity assignments, considerations of matches in excitation energies, and agreement between observed and predicted electromagnetic decay properties. For the levels below about 4 MeV excitation energy there seems little uncertainty in making these correspondences. Up this energy there is a one-to-one correspondence between predicted levels and the observed positive-parity levels. The few levels of negative parity below this energy seem securely assigned and there seems little likelihood that positive-parity levels in this region have escaped detection.

Above 4 MeV excitation energy, however, ambiguities in making correspondences between model and observed states arise from a variety of sources. Some model states are predicted for which experimental counterparts have not been identified. This type of discrepancy can reflect either an incomplete experimental survey or a defect in the model Hamiltonian which creates too high a density of levels per energy interval. The opposite kind of discrepancy, an excess of experimental states over those predicted by the model, is eventually inevitable, even with the ideal model Hamiltonian. States whose quantum numbers are consistent with the model space but which nonetheless originate in excitations which violate the model restrictions on active orbits must be found experimentally in a spectrum at some point of increasing excitation energy. The question is not whether these "intruder" states occur but at what excitation energy they start to appear and how to distinguish them from the "intra-model" states. It can be anticipated that experimental difficulties in finding and characterizing states at higher excitation energies actually disguise the extent of the surplus of "intruder" states over the model level density.

The failure to date of experiments to detect levels which actually exist becomes increasingly conceivable as the rising level density at higher excitation energies makes ever more stringent demands on resolution in the detection of both particles and gamma rays. In addition, states, with J values of 4 and higher, which occur beginning at these excitation energies, may be less easily populated with some conventional reactions, such as the present (p,γ) reaction. For example, the shell-model calculations predict the $(4^+;0)_1$ state to occur at 4593 keV excitation energy, close to the $(5^+;0)_1$ state. The second and third states each with $(J;T)=(5;0)$ and $(4;0)$ are predicted to occur in region of excitation energy 5.1–5.6 MeV. Of these states, only the $(5^+;0)_1$ has been observed, at 4344 keV excitation energy. Based on the singular decay properties

which such states must display, none of the other existing measured states is a good candidate to be one of these missing higher-spin states. The only other state predicted to occur below 5.6 MeV excitation energy for which we have not postulated and experimental counterpart is the $(2;0)_5$ state, at 5471 keV. The fifth $(2^+;0)$ state might be one of the experimentally observed states to which we have assigned another spin-isospin, but this would then leave some alternate model state unaccounted for. Unlike the higher-spin states, there is no particular reason why a state such as the $(2^+;0)_5$ should not be observed. It might have escaped detection or it might be one of the increasing number of states at higher excitation energy which has not received a specific spin-parity assignment. One candidate to correspond to the $(2^+;0)_5$ model state is the unassigned state observed at 5577 keV. This state should have spin of either 2 or 3 on the basis of its decay branches.

The first strong suggestion of an intruder state is the 4941 keV level experimentally assigned $(1^+;0)$. This assignment, together with those of the remainder of the spectrum, cannot be made consistent with the model spectrum of $(1^+;0)$ states. It might be noted that the observed properties of this state are a little peculiar for a $(1^+;0)$ assignment, in that the pure $E2$ decay to the $(3^+;0)$ state must dominate several other possible, nominally more probable, branches. However, the required $E2$ matrix element is not excessively large. In any case, it is highly probable that the region of excitation energy immediately above 5 MeV contains some intruder states even if they are not yet experimentally identified, and that above 6 MeV the density of such states becomes increasingly large relative to the intra-model states.

In summary, the shell-model wave functions of Ref. 6 provide a comprehensive and accurate accounting for all the positive-parity levels below about 5 MeV excitation energy in ^{30}P. Excitation energies are reproduced to within about 150 keV, $E2$ matrix elements to within about 1 $e\,\mathrm{fm}^2$, and $M1$ matrix elements to within about 0.1 μ_N. One of the more than twenty cases studied we find three examples in which the predicted $M1$ matrix elements are significantly larger than the already large experimental values. In another couple of cases the model predicts $M1$ matrix elements of moderate magnitude which significantly exceed the experimental limits. With these exceptions, the theoretical electromagnetic matrix elements agree well with the experimental results. At a level of greater detail, the experimental results indicate a clear preference for the renormalized over the free-nucleon $M1$ operator. While the complexity of the renormalization is such that it affects different matrix elements in different ways, the average effect of the renormalization is to quench $M1$ strength. This conclusion could be drawn much more clearly if more of the experimental measurements resulted in unambiguous measurements of $M1$ strength rather than in upper bounds. Among the various needs for further experimental work to which the present study points, the measurement of additional values of $E2/M1$ mixing ratios would greatly enhance the yield from the existing spin-parity-energy and lifetime measurements.

This work was supported in part by the Academy of Finland and the U.S. National Science Foundation Grant No. PHY-85-09736.

[1]P. Tikkanen, J. Keinonen, V. Karttunen, and A. Kuronen, Nucl. Phys. **A456**, 337 (1986).
[2]R. Lappalainen, J. Keinonen, and A. Luukkainen, Nucl. Phys. **A441**, 1 (1985).
[3]R. Lappalainen, *et al.*, Nucl. Phys. **A426**, 287 (1984).
[4]J. Keinonen, in *Capture Gamma-Ray Spectroscopy and Related Topics—1984* (International Symposium, Knoxville, Tennessee), AIP Conf. Proc. No. 125, edited by S. Raman (AIP, New York, 1985), pp. 557–569.
[5]B. A. Brown, Phys. Rev. C **26**, 2247 (1982).
[6]See B. H. Wildenthal, in *Capture Gamma-Ray Spectroscopy and Related Topics—1984,* Ref. 4, pp. 89–102.
[7]B. A. Brown, in *International Nuclear Physics Conference,* Harrogate, U.K., 1986, IOP Conf. Ser. No. 86, edited by J. L. Durell, J. M. Irvine, and G. C. Morrison (IOP, Bristol, 1986), pp. 119–157.
[8]P. M. Endt and C. van der Leun, Nucl. Phys. **A310**, 1 (1978).
[9]A. Anttila and J. Keinonen, Phys. Rev. C **21**, 1196 (1980).
[10]T. K. Alexander *et al.*, Phys. Rev. Lett. **49**, 438 (1982).
[11]J. P. L. Reinecke *et al.*, Nucl. Phys. **A435**, 333 (1985).
[12]G. I. Harris, A. K. Hyder, and J. Walinga, Phys. Rev. **187**, 1413 (1969).
[13]P. G. Bizzetti *et al.*, Lett. Nuovo Cimento **11**, 775 (1969).
[14]M. Bini *et al.*, Il Nuovo Cimento **4A**, 45 (1971).
[15]A. Lachaine and B. Hird, Can. J. Phys. **48**, 2336 (1970).
[16]J. F. Sharpey-Schafer *et al.*, Nucl. Phys. **A167**, 602 (1971).
[17]P. J. Nolan *et al.*, J. Phys. A **5**, 454 (1972).
[18]E. F. Kennedy, D. H. Youngblood, and A. E. Blaugrund, Phys. Rev. **158**, 897 (1967).
[19]J. Lindhard, M. Scharff, and H. E. Schiøtt, K. Dan. Vidensk. Selsk. Mat.-Fys. Medd. **33**, No. 14 (1963).
[20]Eberhardt *et al.* (unpublished), given as private communication in Ref. 8.
[21]R. Graves and D. K. McDaniels, Bull. Am. Phys. Soc. **14**, 1173 (1969).
[22]R. E. Pixley and A. R. Poletti, Bull. Am. Phys. Soc. **1**, 125 (1969).
[23]A. Luukko, S. Penttinen, A. Anttila, and M. Bister, Phys. Scr. **5**, 63 (1972).
[24]M. Bister, A. Anttila, and J. Keinonen, Phys. Lett. **53A**, 471 (1975).
[25]J. Keinonen, A. Luukkainen, and M. Bister, Nucl. Phys. **A412**, 101 (1984).
[26]J. Keinonen, A. Luukkainen, A. Anttila, and M. Erola, Nucl. Instrum. Methods **216**, 249 (1983).
[27]A. E. Blaugrund, Nucl. Phys. **88**, 501 (1966).
[28]J. H. Ormrod, J. B. Macdonald, and H. E. Duckworth, Can. J. Phys. **43**, 275 (1965).
[29]T. K. Alexander and J. S. Forster, in *Advances in Nuclear Physics,* edited by M. Baranger and E. Vogt (Plenum, New York, 1978), Vol. 10, p. 197.
[30]Comprehensive comparison of experimental and theoretical $M1$ and $E2$ strengths in $A=17$–39 nuclei will be published separately by B. H. Wildenthal and J. Keinonen.